Earth and Planetary Science Letters 312 (2011) 114–125

Contents lists available at SciVerse ScienceDirect

Earth and Planetary Science Letters

journal homepage: www.elsevier.com/locate/epsl

Chromium isotopes in carbonates — A tracer for climate change and for reconstructing the redox state of ancient seawater

R. Frei [a,b,*], C. Gaucher [c], L.N. Døssing [a,b], A.N. Sial [d]

[a] Institute of Geography and Geology, University of Copenhagen, Øster Voldgade 10, 1350 Copenhagen, Denmark
[b] Nordic Center for Earth evolution, NordCEE, University of Copenhagen, Denmark
[c] Departemento de Geología, Facultat de Ciencias, Iguá 4225, 11400 Montevideo, Uruguay
[d] NEG-LABISE, Departemento de Geologia, Universidade Federal de Pernambuco, Brazil

ARTICLE INFO

Article history:
Received 15 June 2011
Received in revised form 27 September 2011
Accepted 3 October 2011
Available online 30 October 2011

Editor: G. Henderson

Keywords:
chromium isotopes
carbonates
chemostratigraphy
Ediacaran
Arroyo del Soldado Group
climate change

ABSTRACT

Strontium and carbon isotopes of marine carbonates are routinely applied for chemostratigraphic cross correlations of time-equivalent sedimentary sequences and for calibration of the compositional evolution of seawater throughout Earth's history, mainly for the purpose of reconstructing ancient climatic changes. We here present results of a new isotopic tracer system – stable chromium isotopes – applied to a late Ediacaran marine carbonate sequence exposed in the Calera de Recalde syncline, Arroyo del Soldado Group, Uruguay. The aim was to compare Cr isotope signatures directly to $\delta^{13}C$, $^{87}Sr/^{86}Sr$ and $^{143}Nd/^{144}Nd$ fluctuations in a well defined stratigraphic profile comprising sediments that were deposited during cold–warm periods accompanied by sea-level changes in response to glaciation–deglaciation at higher latitudes. The studied section is characterized by a pronounced negative (down to −3.3‰) $\delta^{13}C$ excursion in carbonates paralleled by a decrease of $^{87}Sr/^{86}Sr$ values. Chromium isotope signatures over this section also show a correlated decrease in $\delta^{53}Cr$ ($\delta^{53}Cr = [((^{53}Cr/^{52}Cr)_{sample}/(^{53}Cr/^{52}Cr)_{SRM979}) - 1] \times 1000$) values from ~+0.29 to −0.17‰ which mirrors a decrease in positively fractioned seawater signatures to slightly negative values characteristic of high-temperature magmatic sources. Linear correlations between $\delta^{53}Cr$ and εNd(570 Ma), $^{87}Sr/^{86}Sr$ and Cr concentrations can be explained by mixing between two major input sources of Cr, Nd and Sr into the shallow seawater: 1) a source characterized by negative $\delta^{53}Cr$ values of ~−0.2‰, low $^{87}Sr/^{86}Sr$ values of ~0.707, and elevated $^{147}Sm/^{144}Nd$ values of ~0.13, recognized as a subaqueous hydrothermal dominated input source, and 2) a source characterized by positively fractionated $\delta^{53}Cr$ values of ~+0.2‰, higher $^{87}Sr/^{86}Sr$ values of ~0.708, and lower $^{147}Sm/^{144}Nd$ values of ~0.11, a source which is strongly affected by continentally derived input. Chromium isotopes provide a powerful tool for reconstructing the redox state of ancient seawater since positive values indicate that, at least locally, Neoproterozoic shallow ocean waters were sufficiently oxidized to fractionate chromium and/or that oxygen levels of the atmosphere were sufficient to transform Cr(III) into the more mobile hexavalent Cr(VI) formed during weathering processes on land.
The fact that $^{87}Sr/^{86}Sr$ values, despite $\delta^{13}C$ fluctuations, remain low (indicative of a strong hydrothermal input into the basin at his time) implies that CO_2 limitation was the cause of negative $\delta^{13}C$ and $\delta^{53}Cr$ excursions in otherwise nutrient rich late Neoproterozoic basins, and that glaciation is only one more consequence of a tectonically driven, biologically mediated system. In such a scenario, glaciation acts as an amplifier of $\delta^{53}Cr$ signals. These signals in marine carbonates are a sensitive tracer for redox processes in the ocean and/or on land and have the potential to contribute significantly, in combination with the other commonly used isotopic tracers, to the reconstruction of climatic changes, particularly those that are associated with major glaciation periods in Earth's history.

1. Introduction

The major agent of Cr(III) oxidation in soils and sediments is manganese oxides (Kim et al., 2002; Oze et al., 2007), but little is known about the effects accompanying Cr(III) oxidation. Cr(III) oxidation by the Mn-oxide birnessite (δ-MnO_2) revealed wide variations in $\delta^{53}Cr$ values of the developing Cr(VI) pools between −2.5 and +0.7‰ (Bain and Bullen, 2005) and little enrichment (<~+0.2‰) of the oxidized Cr(VI) pools under a variety of prevailing pH values was demonstrated by Zink et al. (2010). The highly variable positive and negative isotope fractionation during the overall process of Cr oxidation has been interpreted by these authors to derive from partial back-reduction of instable intermediates Cr(IV) and Cr(V). Reduction of Cr(VI) to Cr(III) has shown to be

* Corresponding author at: Institute of Geography and Geology, University of Copenhagen, Øster Voldgade 10, 1350 Copenhagen K, Denmark. Tel.: +45 35 32 24 50; fax: +45 35 32 25 01.
E-mail address: robertf@geo.ku.dk (R. Frei).

0012-821X/$ – see front matter © 2011 Elsevier B.V. All rights reserved.
doi:10.1016/j.epsl.2011.10.009

extremely effective on the surface of Fe(II)-bearing minerals (Døssing et al., 2011; Ellis et al., 2002), and this process is being efficiently used to decontaminate surface and groundwaters from toxic Cr(VI). While it seems that oxidation of Cr(III) to Cr(VI) only causes limited Cr isotope fractionation of maybe 0.1 to 0.2‰, partial back reduction of the oxidized and soluble Cr(VI) in natural aquifers seems to cause a large isotope fractionation. This is exemplified by the studies of Berna et al. (2010) and is corroborated by the observation that the Cr isotopic composition of soluble Cr(VI) in the anthropogenically uncontaminated groundwater of the western Mojave desert has exclusively positive δ^{53}Cr values between +0.7 and +5.1‰ (Izbicki et al., 2008).

In contrast, a survey of the stable chromium isotopic compositions of igneous Earth reservoirs reveals a very narrow range in δ^{53}Cr of -0.124 ± 0.101‰ (Schoenberg et al., 2008). Chromium in igneous terrestrial reservoirs is present in the trivalent oxidation state, and the release of Cr(III) from solid rocks through chemical weathering or by hydrothermal systems at mid-ocean ridges is not expected to cause significant Cr isotope fractionation.

Chromium isotopes have proved powerful in reconstructing the redox state of ancient seawater (Frei et al., 2009). The redox-coupled (Cr(III) to Cr(VI)) release of chromium from the continents is, among other parameters, dependent on the oxygenation state of the atmosphere. Because this release is accompanied by an isotopic fractionation preferentially enriching the heavier isotopes in the mobilized Cr(VI), chromium isotopes in surface seawater have the potential to indirectly trace climatic changes linked to fluctuations of atmospheric oxygen. Cr(VI) is the thermodynamically stable form in seawater (as CrO_4^{2-}) with lower amounts (5–20%) of Cr(III) in modern surface seawaters (Connelly et al., 2006). Chromium isotopes in Fe-rich chemical sediments (banded iron formations; BIFs) record the redox state of ancient seawater, whereby the signal from surface seawater is effectively conveyed into the Fe-rich chemical sediment through interaction of upwelling Fe-rich bottom waters with oxygenated surface waters. In such a process, chromium is concomitantly co-precipitated with Fe-oxihydroxides (Døssing et al., 2011). Positively fractionated chromium values have notably been observed in BIFs that were deposited during the Archean/Proterozoic boundary (Great Oxidation Event; GOE) and during the Late Neoproterozoic (Neoproterozoic Oxidation Event; NOE). The close temporal relationship between positive δ^{53}Cr excursions recorded in BIFs and warm periods following major Precambrian glaciation events make it likely that these isotope signals monitor climatic changes in local and/or regional “Snowball Earth” or “Slushball Earth” scenarios (Frei et al., 2009).

We explore here the promise for preservation of a shallow seawater chromium isotope signal in carbonates as a further archive to record redox states of ancient seawater and to trace climatic changes through Earth's history. Recently reported results from five international natural carbonate reference materials revealed δ^{53}Cr values that range from +0.74 to +2.00‰ (Bonnand et al., 2011). Bonnand et al. (2010) also analyzed the Cr isotope composition of modern seawater and reported heavy δ^{53}Cr values of ~+0.5‰. The δ^{53}Cr value of modern seawater is comparable to δ^{53}Cr values of +0.6 to +0.8‰ which these authors determined on ooids from the Bahamas Bank. These positively fractionated chromium values are compatible with our own unpublished data on modern iron oolites from a shallow-marine volcanic setting (Mahengetang, Indonesia; Heikoop et al. (1996)) with δ^{53}Cr values of +0.6‰.

We apply in this study δ^{53}Cr, δ^{13}C, ^{87}Sr/^{86}Sr and Nd isotopes to a well-studied late Ediacaran carbonate succession: the lower Arroyo del Soldado Group. The Yerbal Formation and especially the overlying Polanco Formation are the focus of this study, because they record distinct δ^{13}C oscillations associated to eustatic sea-level variations, microfossil diversity changes and redox fluctuations (Gaucher et al., 2004b; Gaucher et al., 2009; Velasquez, 2010). The Yerbal and Polanco formations are also fossiliferous (e.g. Gaucher and Poiré (2009a)) and bear distinct BIF horizons that yielded positive δ^{53}Cr values, which make these units interesting in order to reveal the relationship between late Neoproterozoic climatic oscillations, extinction and radiation events, ocean chemistry and changes in atmospheric oxygenation (e.g. Canfield et al., 2008; Frei et al., 2009; Johnston et al., 2010).

2. Geological relationships

The Arroyo del Soldado Group (ASG) crops out over an area in excess of 30,000 km^2 in the Nico Pérez Terrane (NPT), a block accreted to the Rio de la Plata Craton at 1.25 Ga (Bossi and Cingolani, 2009; Fig. 1). The NPT is bounded by two continental-scale megashears, the Sarandí del Yí Shear Zone (SYSZ) and the Sierra Ballena Shear Zone (SBSZ; Fig. 1). The ASG represents a marine platform succession more than 5000 m thick (Gaucher, 2000) which unconformably overlies Archean and Proterozoic rocks of the NPT. The unit is composed, from base to top, by the Yerbal, Polanco, Barriga Negra, Cerro Espuelitas, Cerros San Francisco and Cerro Victoria Formations (Gaucher, 2000). The lithostratigraphy of the ASG has been described in detail by Gaucher and coworkers (Gaucher, 2000; Gaucher et al., 2004a, 2004b; Gaucher et al., 2007; Gaucher et al., 2008a) and a summary is contained in the supplementary information.

2.1. Age and evolution of the Arroyo del Soldado Group

The ASG is folded, fault-bounded and intruded by several plutons of Cambrian age (Fig. 1). The ASG was affected by late diagenesis to anchimetamorphism, with maximum paleotemperatures of 200 °C (Gaucher, 2000). The ASG overlies the Mangacha Granite, for which Gaucher et al. (2008b) reported a U–Pb SIMS age of 583 ± 7 Ma. The Las Ventanas Formation, a rift succession which hosts glacial deposits of Gaskiers age, also pre-dates the ASG (Gaucher et al., 2008a). Deposition of the Las Ventanas Formation is bracketed between 590 ± 2 Ma and 573 ± 11 Ma (Gaucher et al., 2008a; Mallmann et al., 2007; Oyantcabal et al., 2009). A further maximum age constraint is provided by a U–Pb LA-ICP-MS age of 566 ± 8 Ma for the youngest detrital zircon in the Barriga Negra Formation (Gaucher et al., 2008b). The occurrence of the skeletal fossil *Cloudina riemkeae* in the Yerbal and Polanco formations along with well-preserved acritarch assemblages indicates a late Ediacaran age for the lower and middle ASG (Gaucher, 2000; Gaucher and Poiré, 2009a). C-, O-, and Sr-isotopic data also support a late Ediacaran age for the Yerbal, Polanco, Barriga Negra and Cerro Espuelitas Formations and a Lower Cambrian age for the Cerros San Francisco and Cerro Victoria Formations (Gaucher et al., 2004b; Gaucher et al., 2007; Gaucher et al., 2009). Thus, deposition of ASG took place between *ca.* 565 and 535 Ma. On the basis of litho-, bio- and chemostratigraphic data, the ASG can be correlated with other Neoproterozoic–Early Paleozoic successions of South America (Corumbá Group in Mato Grosso in Brazil) (Boggiani et al., 2010; Gaucher et al., 2003); Sierras Bayas Group, Argentina (Gaucher and Poiré, 2009b; Gaucher et al., 2005) indicating a large shelf margin along the eastern side of the Río de la Plata Craton (Gaucher et al., 2003; Gaucher et al., 2008b).

2.2. Chemostratigraphy of the lower Arroyo del Soldado Group

Gaucher et al. (2004b) and Gaucher et al. (2009) present C- and O-isotopic data for the lower Arroyo del Soldado Group. The δ^{13}C curve of Gaucher et al. (2009) is depicted in Fig. 3. Positive δ^{13}C values characterize the mainly siliciclastic upper Yerbal Formation, which contains oxide-facies BIF and a diverse assemblage of skeletal fossils, including *Cloudina riemkeae*. A series of positive and negative δ^{13}C excursions occur up-section in the overlying Polanco Formation, mainly composed of limestones and limestone–dolostone rhythmites. Positive δ^{13}C excursions were interpreted to be associated with high sea-level stand, high organic carbon burial and relatively higher microfossil diversity, whereas negative δ^{13}C excursions occur in carbonates with less organic matter and less microfossil diversity, and are

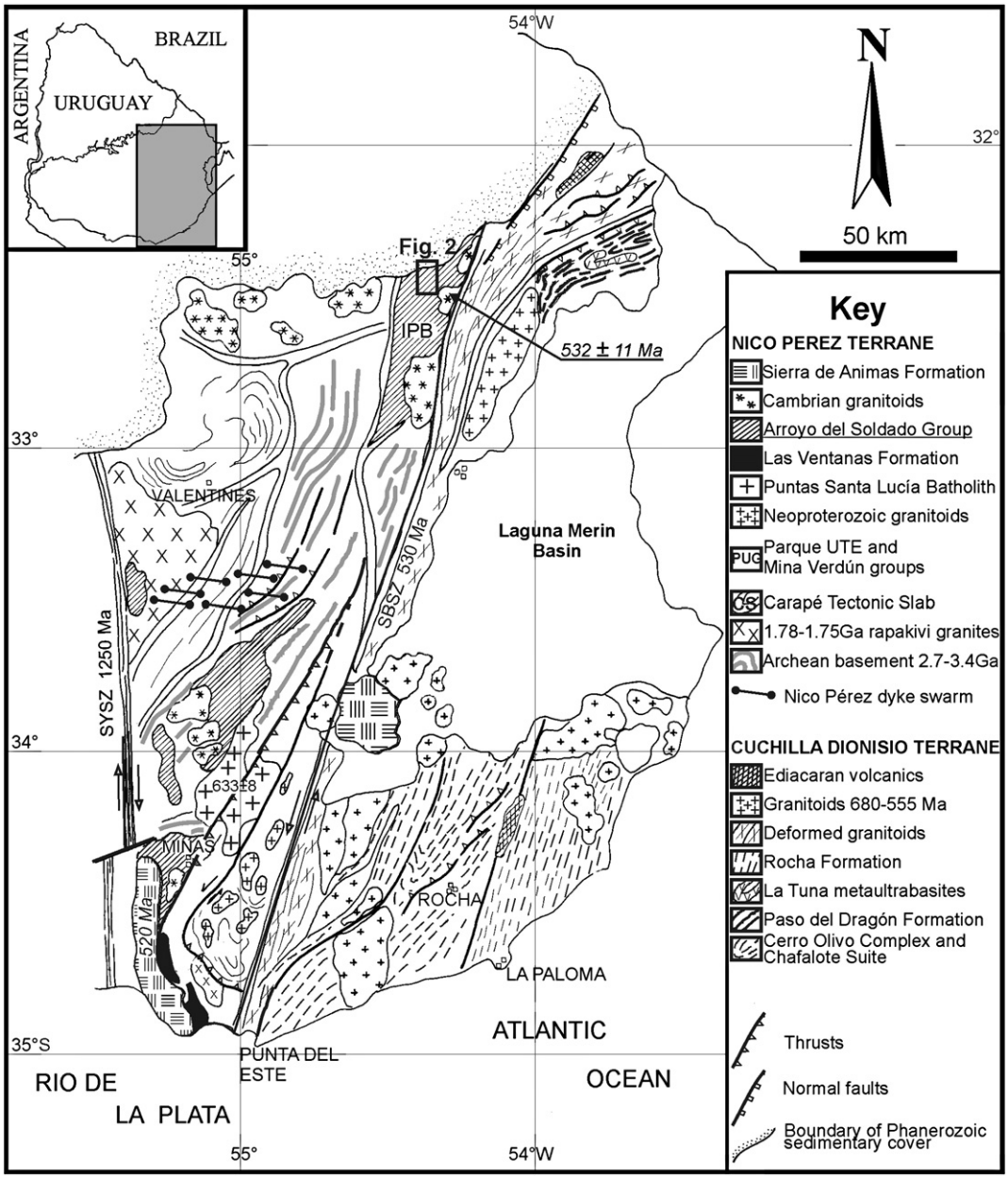

Fig. 1. Geological sketch-map of the Nico Pérez and Cuchilla Dionisio terranes in Uruguay, showing the geographic distribution of the late Ediacaran to basal Cambrian Arroyo del Soldado Group and the location of the studied area (shown in Fig. 2) Modified from (Bossi and Gaucher, 2004). IPB = Isla Patrulla Block; SYSZ = Sarandí del Yí-Piriápolis Shear zone; SBSZ = Sierra Ballena Shear Zone.

associated with low sea-level (Gaucher, 2000; Gaucher et al., 2004b). The detailed stratigraphic column comprising the uppermost Yerbal and Polanco Formations in the Calera de Recalde Syncline profile (Figs. 2 and 3) studied by Gaucher and coworkers (Gaucher et al., 2004b; Gaucher et al., 2009) revealed the occurrence of two regressions characterized by negative $\delta^{13}C$ excursions, interpreted as the result of non-global glacial events. The absence of glaciogenic rocks associated with these negative $\delta^{13}C$ excursions in the ASG is probably due to the tropical setting of the basin (Gaucher et al., 2004b).

The most impressive negative $\delta^{13}C$ excursion recorded in the whole ASG is represented by the middle Polanco N1 excursion, comprising 200 m of carbonates, which has been correlated with the Shuram–Wonoka anomaly (Boggiani et al., 2010; Gaucher et al., 2009). Sr isotope values also reach a nadir during the N1 excursion, possibly indicating tectonic forcing of the carbon cycle (Gaucher and Poiré, 2009b). Velasquez (2010) showed that redox-sensitive elemental ratios (e.g. U/Th, V/Th), Ce anomaly magnitudes and rare-earth concentrations all point to an anoxic water column during N1, in contrast to the underlying, $\delta^{13}C$-positive carbonates (P1).

According to the model put forward by Gaucher et al. (2004b), carbonates deposited during the P1 positive excursion record a warm phase characterized by high plankton bioproductivity and eutrophic conditions fueled by high nutrient input. The co-occurring, low-diversity acritarch assemblage, dominated by the genera *Bavlinella* and *Soldadophycus*, corroborates this (Gaucher, 2000; Gaucher and Poiré, 2009b). The overlying N1 negative excursion was interpreted on the basis of sedimentary structures as a regression caused by glaciation at higher latitudes, which explains also the negative $\delta^{13}C$ values that suggest biotic stress. Warm, high-productivity, eutrophic conditions return in the overlying P2 positive $\delta^{13}C$ excursion. The ultimate driver of these oscillations may have been global tectonics, as evidenced by associated $^{87}Sr/^{86}Sr$ oscillations (Gaucher et al., 2009).

The observed fluctuations in redox conditions, carbon-isotope composition of seawater and Sr-isotope ratios prompted us to apply

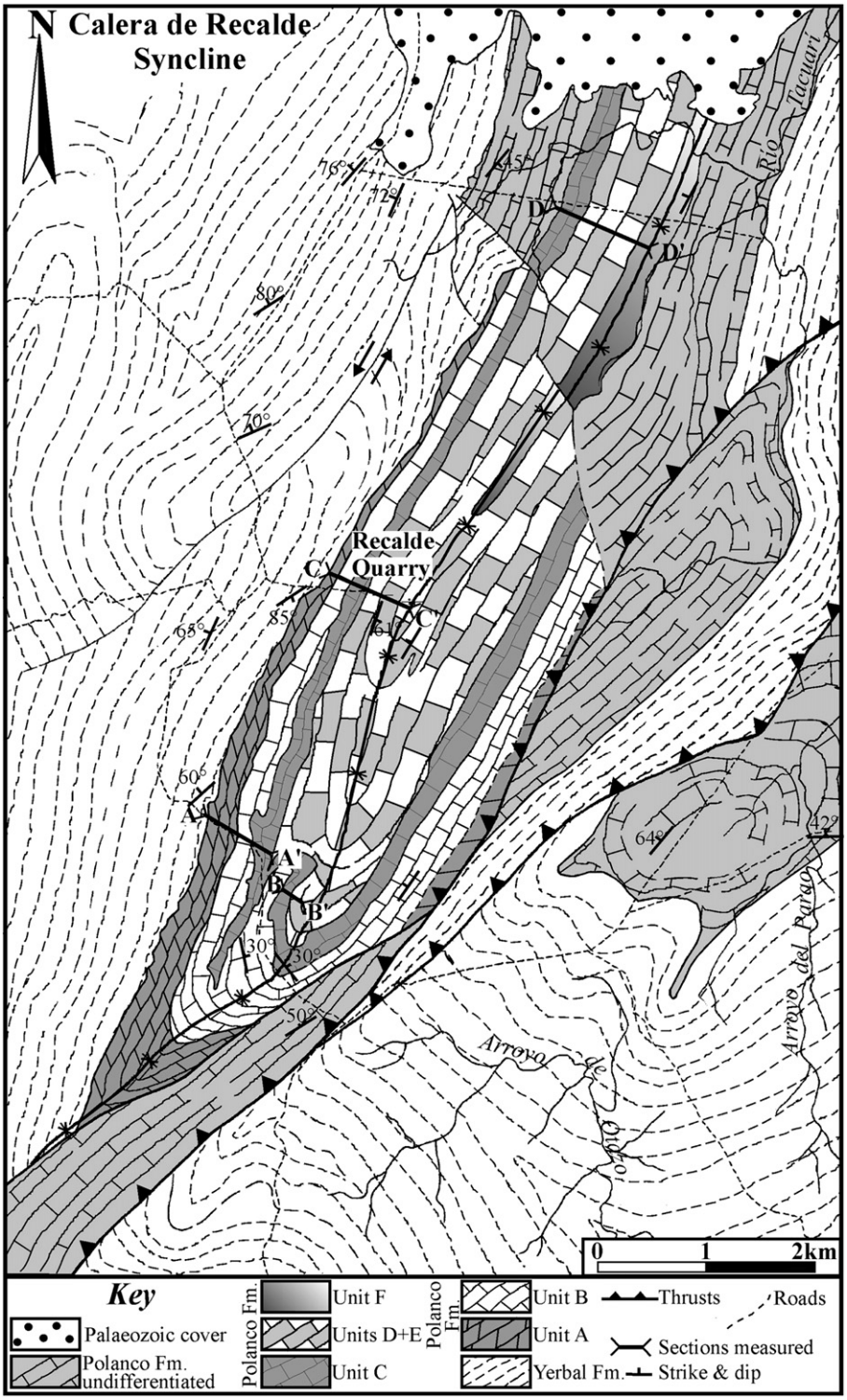

Fig. 2. Geological map of the Calera de Recalde Syncline, showing different units within the Polanco Formation (from Gaucher et al., 2004b). Sections AA′, BB′, CC′ and DD′ were studied and are summarized in the stratigraphic column shown in Fig. 3.

the Cr isotope system to the Polanco Formation in order to test the idea of fluctuating oxygen concentrations in phase with large-scale carbon isotope excursions in the Arroyo del Soldado basin.

3. Material and methods

A detailed description of the analytical procedures is contained in the supplementary information accompanying this article. We here present a summary of these details.

3.1. Purification of Sr, Nd and Cr

Powdered samples weighing between 100 mg and 1 g were doped with an adequate amount of Cr double spike. Detailed specifications of the double spike are contained in Døssing et al. (2011). Afterwards, the samples were attacked by 0.5 to 5 mL of 0.5 mol L^{-1} acetic acid for 10 min in an attempt to liberate Cr from calcite only (see Supplementary information). After centrifugation the supernatant was pipetted off into a 7 mL Savillex™ Teflon beaker and placed on a hot

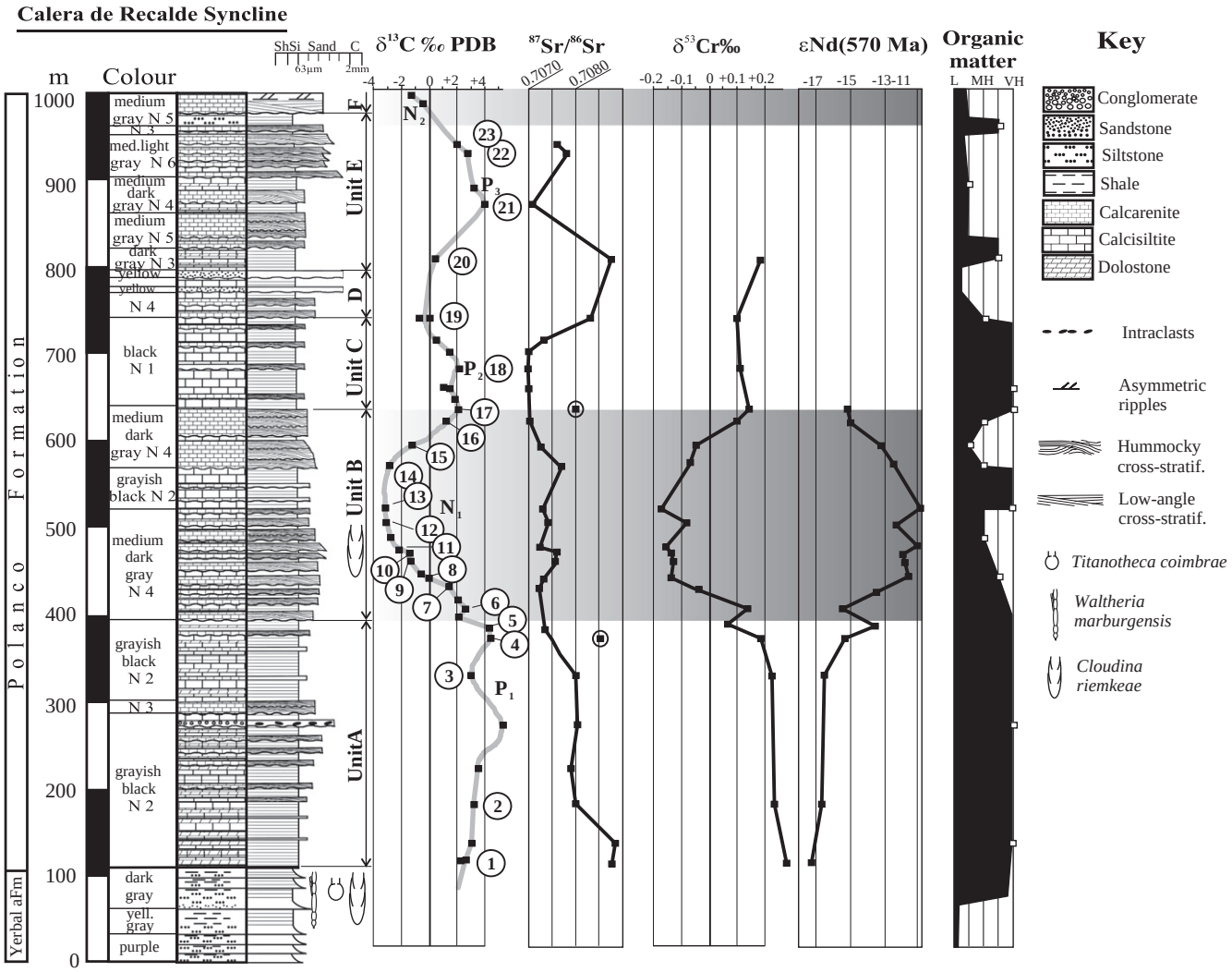

Fig. 3. Detailed stratigraphic column of the Polanco and uppermost Yerbal formations and corresponding $\delta^{13}C$ with relative organic matter content (L = low; MH = medium-high; VH = very high), modified and expanded from Gaucher et al. (Gaucher et al., 2004b; Gaucher et al., 2009). Chromium ($\delta^{53}Cr$), $^{87}Sr/^{86}Sr$ and εNd(570 Ma) isotope data from this study are added as separate columns. Encircled black squares in the $^{87}Sr/^{86}Sr$ log denote diagenetically altered samples. Number-labeled data points in the $\delta^{13}C$ log correspond to numbers in Table 1. N1 depicts a major negative $\delta^{13}C$ excursion that has been correlated with similar features in China, Brazil and Namibia (see text for details). The negative (N1) $\delta^{13}C$ excursion is concomitant to a decrease of $\delta^{53}Cr$ values and both are preceded by a decrease in $^{87}Sr/^{86}Sr$ ratios, illustrating the potential of chromium isotopes in carbonates to monitor climatic changes (see text for details).

plate at 130 °C with a closed lid overnight. After drying down the solution, the samples were taken up in 3 mL of 6 mol L^{-1} HCl and were then subjected to anion chromatography to separate Cr from matrix elements using a method similar to that described by Frei et al. (2009).

Twenty milligrams of powdered carbonate was added to a 2 mL polypropylene centrifuge tube and exposed to 1 mL of 0.5 mol L^{-1} acetic acid for 10 min. The solution was centrifuged and the supernatant pipetted off into a 7 mL Savillex™ Teflon beaker and dried down. Samples were taken up in a few drops of 3 mol L^{-1} HNO_3 and then loaded on commercially available (Eppendorf ™) 1 mL pipette tips with a pressed-in filter designed to be used as an extraction column. These columns were charged with 200 µL of an intensively precleaned mesh 50–100 SrSpec™ (Eichrome Inc./Tristchem) resin. The elution recipe followed that of Horowitz et al. (1992). Strontium was eluted/stripped by pure deionized water.

Two hundred milligrams of carbonate powder was added to an adequate amount of mixed ^{149}Sm–^{150}Nd spike and attacked by 2 mL of 0.5 mol L^{-1} acetic acid for 10 min. The supernatant was dried down and the solid was taken up in 300 µL of 2 mol L^{-1} HCl. Ion chromatographic separation took place first over a cation exchange column (separation of bulk REE), then over a column charged with Eichrom/Trischem's Ln-resin (to separate REE from each other) according to the procedure described by Kalsbeek and Frei (2010).

3.2. TIMS measurements

Chromium, Sr and Sm–Nd isotope measurements were made on an IsotopX/GV IsoProbeT thermal ionization mass spectrometer (TIMS). Amounts of ~1–2 µg of Cr were loaded onto Re filaments with a mixture of 3 µL silica gel, 0.5 µL 0.5 mol L^{-1} of H_3BO_3 and 0.5 µL 0.5 mol L^{-1} of H_3PO_4. The samples were measured at a temperature of 980–1100 °C, aiming for a beam intensity at atomic mass unit (AMU) 53 of 30–60 mV. Every load was analyzed 2–4 times (see Table 1). Titanium, vanadium and iron interferences with Cr isotopes were corrected by comparing with $^{49}Ti/^{50}Ti$, $^{50}V/^{51}V$ and $^{54}Fe/^{56}Fe$ ratios. The final isotope composition of a sample was determined as the average of the repeated analyses and reported relative to the certified SRM 979 standard as

$$\delta^{53}Cr(‰) = \left[\left(^{53}Cr/^{52}Cr_{sample}/^{53}Cr/^{52}Cr_{SRM\ 979}\right) - 1\right] \times 1000$$

Repeated analysis of 1.5 μg loads of unprocessed double spiked NIST SRM 3112a standard yielded a 2σ external reproducibility in δ^{53}Cr value of ±0.05‰ (^{52}Cr signal intensity of 1 V) and of ±0.08‰ (^{52}Cr beam intensity of 500 mV).

Strontium samples were dissolved in 2.5 μl of a Ta_2O_5–H_3PO_4–HF activator solution and loaded directly on to previously outgassed 99.98% single rhenium filaments. Samples were measured at 1250–1300 °C in dynamic multi-collection mode. Fifty nanogram loads of the NBS 987 Sr standard gave $^{87}Sr/^{86}Sr = 0.710236 \pm 0.000010$ ($n = 14$, 2σ). The $^{87}Sr/^{86}Sr$ values of the samples were corrected for the offset relative to the certified NIST SRM 987 value of 0.710250. The errors reported in Table 1 are within-run ($2\sigma_m$) precisions of the individual runs.

Sm–Nd isotopes were analyzed applying both static (Sm) and multidynamic (Nd) routines for the collection of the isotopic ratios. Nd isotope ratios were normalized to $^{146}Nd/^{144}Nd = 0.7219$. The mean value of $^{143}Nd/^{144}Nd$ for the JNdi-1 standard (Tanaka et al., 2000) during the period of measurement was 0.512109 ± 0.000009 ($n = 5$; 2σ).

4. Results

Samarium–neodymium, Sr and Cr isotopic ratios and their elemental concentrations in carbonates collected over the N1 negative carbon isotope excursion (Fig. 3) are contained in Table 1. Chromium

Table 1
Sm–Nd, Sr and Cr isotope data of carbonates from Calera de Recalde (Polcanco Formation; Arroyo del Soldado Group, Uruguay).

Sample	Rock description	Label[a]	Unit	Sm (ppm)	Nd (ppm)	$^{147}Sm/^{144}Nd$	$^{143}Nd/^{144}Nd$	±2σ mean (%)	εNd (0)	εNd (570)	$^{143}Nd/^{144}Nd_{ini}$	$^{87}Sr/^{86}Sr$	$\delta^{13}C$[b]	Cr[c] (ppm)	$\delta^{53}Cr_{average}$ (‰)	$\pm 2\sigma_m$[d]	n[f]
0001116-1	Calcisiltite from rhythmite	1	A	0.97	5.61	0.10442	0.511413	0.00011	−23.9	−17.2	0.511023	0.70878	0.4	20.3	0.29	0.05	2
0001116-2	Calcisiltite from rhythmite	2	A	1.56	9.19	0.10906	0.511454	0.00012	−23.1	−16.7	0.511047	0.70795	3.0	25.1	0.25	0.05	4
0001117-4	Calcisiltite	3	A	1.03	5.49	0.11729	0.511497	0.00020	−22.3	−16.5	0.511059	0.70812		11.7	0.22	0.03	4
0001117-5[e]	Fine calcarenite	4	A	0.66	3.43	0.11568	0.511553	0.00010	−21.2	−15.3	0.511121	0.70854		15.1	0.19	0.06	1
CCU-45 K	Calcisiltite	5	A	0.38	1.95	0.11879	0.511647	0.00039	−19.3	−13.7	0.511203	0.70731	4.3	14.0	0.06	0.05	2
CCU-45 I	Dolomitic calcisiltite	6	B	0.65	3.59	0.10909	0.511516	0.00008	−21.9	−15.5	0.511109	0.70788	2.7	10.2	0.14	0.05	2
CCU-45 F	Dolomitic calcarenite	7	B	1.05	5.62	0.11616	0.511648	0.00011	−19.3	−13.5	0.511214	0.70729	1.4	12.6	−0.07	0.06	2
CCU-45 E	Dolomitic calcarenite	8	B	1.72	8.98	0.11569	0.511738	0.00008	−17.6	−11.7	0.511306	0.70735	−0.1	4.4	−0.13	0.06	2
CCU-45 C	Fine calcarenite	9	B	3.75	16.54	0.12874	0.511769	0.00010	−17.0	−12.0	0.511288	0.70762	−1.2	4.2	−0.12	0.04	2
CCU-45 A	Dolomitic calcarenite	10	B	1.70	7.72	0.12823	0.511745	0.00009	−17.4	−12.4	0.511266	0.70756	−1.3	4.1	−0.13	0.06	2
0001117-6	Dolomitic calcisiltite	11	B	0.47	2.23	0.12842	0.511821	0.00012	−15.9	−11.0	0.511342	0.70723	−2.5	2.3	−0.15	0.06	2
0001117-7	Very fine calcarenite	12	B	1.14	4.67	0.12596	0.511733	0.00016	−17.7	−12.5	0.511262	0.70764	−3.1	3.3	−0.07	0.03	2
0001117-8	Calcisiltite from rhythmite	13	B	1.01	5.02	0.12175	0.511808	0.00010	−16.2	−10.7	0.511354	0.70730	−3.3	5.3	−0.17	0.08	2
0001117-9	Calcarenite from rhythmite	14	B	2.15	9.07	0.12751	0.511742	0.00009	−17.5	−12.5	0.511266	0.70774	−2.8	7.4	−0.08	0.03	1
0001117-13	Fine calcarenite	15	B	0.99	5.27	0.11744	0.511670	0.00011	−18.9	−13.1	0.511231	0.70722	−1.0	10.6	−0.06	0.02	4
0001117-14	Calcisiltite	16	B	1.16	5.84	0.12047	0.511585	0.00009	−20.5	−15.0	0.511135	0.70769	1.3	13.8	0.10	0.03	1
0001117-10[e]	Dolosiltite from rhythmite	17	B	1.54	7.42	0.12045	0.511576	0.00011	−20.7	−15.2	0.511126	0.70813	2.1	15.4	0.14	0.01	4
001117-16	Very fine calcarenite	18	C									0.70696	2.1	5.3	0.11	0.05	2
001117-17	Calcisiltite from rhythmite	19	C									0.70830	−0.7	10.4	0.10	0.06	2
001015-5	Dolomitic calcisiltite	20	E									0.70874	0.4	16.4	0.19	0.06	1
020130/6	Calcisiltite	21	E									0.70707	4.1				
020130/3A	Calcisiltite	22	E									0.70698	1.4				
020130/3B	Medium-coarse calcarenite	23	E									0.70729	0.5				

[a] Labels correspond to those in Fig. 3.
[b] Gaucher et al. (2003, 2004).
[c] Concentrations calculated by double spike isotope dilution.
[d] Two standard error of the mean of number (n) of mass spectrometrical runs of an individual sample.
[e] Diagenetically altered, not included in Fig. 3.
[f] Number of mass spectrometrical runs.

and Sr isotope data and εNd (570 Ma) values are plotted along the profile in Fig. 3 and complement the $\delta^{13}C$ curve and the column with organic matter content (Gaucher et al., 2004a; Gaucher et al., 2004b). A comparison of the different curves in Fig. 3 reveals the following relationships:

(1) The N1 negative $\delta^{13}C$ excursion is mirrored by a negative $\delta^{53}Cr$ excursion. Importantly, whereas slightly positive $\delta^{53}Cr$ values of around +0.2‰ characterize carbonates deposited before and after the N1 $\delta^{13}C$ excursion, negatively fractionated values of around −0.1 to −0.2‰ are characteristic of carbonates deposited during N1 excursion.
(2) εNd(570 Ma) values define a log distribution curve which is a near perfect mirror image of the $\delta^{53}Cr$ curve, with values below −15 before and after the N1 $\delta^{13}C$ excursion, and with values between −11 and −15 within the N1 section of the profile.
(3) $^{87}Sr/^{86}Sr$ values are constant around 0.7080 in the P1 excursion (unit A) and decrease to 0.7073 in the uppermost unit A, about 50 m stratigraphically below the onset of the N1 (unit B; Fig. 3) excursion. Sr isotope ratios (with a few exceptions) remain low with values ranging between ~0.7070 and 0.7073 within unit B (N1 negative excursion) and remain consistently low in the overlying unit C (Fig. 3), which records a second positive $\delta^{53}Cr$ excursion (P2).

Results of carbonate samples from which we have the complete data sets (samples from unit A and B; Fig. 3) are plotted in Fig. 4a–d. In Fig. 4a, $\delta^{53}Cr$ values are positively correlated with $^{87}Sr/^{86}Sr$ ratios ($R^2 = 0.5$), and, in Fig. 4b, $\delta^{53}Cr$ data are inversely correlated with εNd (570 Ma) values ($R^2 = 0.9$), mirroring the opposite log curves of these two parameters in Fig. 3. The inter-relationships between $^{87}Sr/^{86}Sr$ and εNd(570 Ma) values are depicted in Fig. 4c, where data are inversely correlated ($R^2 = 0.6$). Similarly, however less pronounced ($R^2 = 0.3$), an inverse correlation also exists between $^{87}Sr/^{86}Sr$ ratios and $^{147}Sm/^{144}Nd$ ratios (Fig. 4d). Scandium concentrations (not reported herein) are throughout <2 ppm, indicating that potential detrital (lithogenic) input into the sediments was subordinate. Finally, we also observe a positive correlation between Cr concentrations and respective $\delta^{53}Cr$ values (depicted in Fig. 5). This systematic relationship is apparently unrelated to detrital input (as mentioned above, here corroborated by a lack of correlation ($R^2 = 0.03$) between Sc and Cr concentrations; diagram not shown herein).

5. Discussion

5.1. Cr isotopes

$\delta^{53}Cr$ values measured on the Ediacaran carbonates of the Polanco Formation vary between −0.17 and +0.29‰ (Table 1), confirming the relatively light Cr isotope composition of Neoproterozoic carbonates (Bonnand et al., 2010). However, our study of a continuous section of carbonates reveals that the apparently narrow range of $\delta^{53}Cr$ found shows well-defined correlations with other tracers (Fig. 4a–d; discussed below). In addition to the very sparse published Cr isotope data of carbonates, data presented herein (in particular positively fractionated $\delta^{53}Cr$ values) indicate that natural carbonates have the potential to record redox oscillations in palaeo-oceans. This observation corresponds to the occurrence of positive $\delta^{53}Cr$ values in BIFs

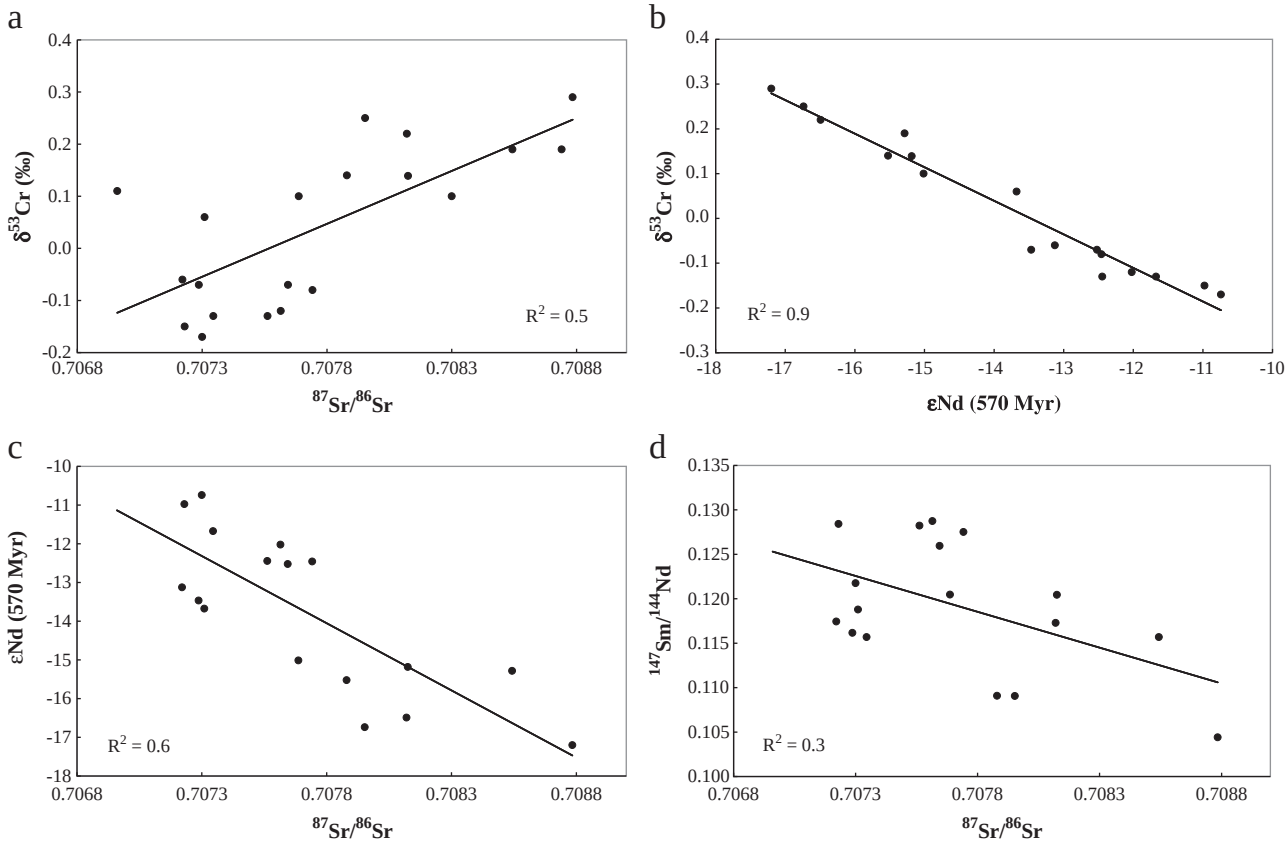

Fig. 4. Correlation diagrams for the carbonates from the Calera de Recalde Syncline profile. a) Diagram showing the relationship between $^{87}Sr/^{86}Sr$ ratios and $\delta^{53}Cr$ values; b) diagram illustrating the εNd(570 Ma) with $\delta^{53}Cr$ relationship; c) diagram showing the correlation between $^{87}Sr/^{86}Sr$ ratios and εNd(570 Ma), and d) diagram demonstrating the relationship between $^{87}Sr/^{86}Sr$ and $^{147}Sm/^{144}Nd$ ratios. The different correlations (coefficient of correlations R^2 indicated in the diagrams) are indicative of a predominant mixing between deep water sourced hydrothermal fluids with lower $^{87}Sr/^{86}Sr$ ratios, less negative εNd(570 Ma) values, and high temperature magmatic, negatively fractionated $\delta^{53}Cr$ values, with shallow seawater characterized by elevated $^{87}Sr/^{86}Sr$ ratios, more negative εNd(570 Ma) values, and by positively fractionated $\delta^{53}Cr$ values typically characterizing a continental crust origin (see text for details).

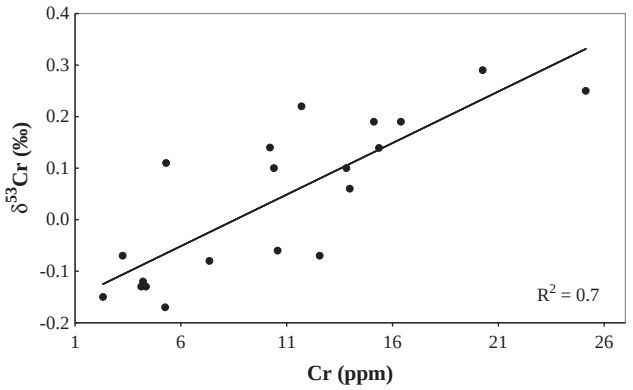

Fig. 5. Diagram illustrating the relationship between chromium concentrations and δ^{53}Cr values of the Calera de Recalde Syncline carbonates. The positive correlation ($R^2 = 0.7$) implies that dissolved, positively fractionated chromium was more concentrated in the shallow seawater during warm periods whereas low chromium concentrations with high-temperature magmatic δ^{53}Cr values prevailed during the cold periods (see text for details).

(Frei et al., 2009). Frei et al. (2009) interpreted the positive δ^{53}Cr values recorded in Precambrian BIFs to indicate the presence of mobilized Cr(VI), and thus the existence of chromium which underwent a process of redox-cycling on land during oxidative weathering. In such a scenario, oxidation of relatively immobile Cr(III) in oxides and silicates of crustal minerals to mobile Cr(VI) would be accompanied by an isotope fractionation which is characterized by release of heavier chromium from the continent into the aqueous phase. Despite possible mechanisms during transport which could back-reduce the mobile and heavy Cr(VI) fractions and thereby rendering Cr immobile again, the presence of positively fractionated Cr isotopes in modern seawater (Bonnand et al., 2010) can, at this point, be taken as an indication for the operation of redox process(es) during the release of Cr (by oxidative weathering processes on land promoted by a strongly oxidative atmosphere) and/or during its transport into the sea. This is corroborated by the positively fractionated recent oolitic limestones from the Bahamas (Bonnand et al., 2010) and our own (unpublished) δ^{53}Cr value of +0.62‰ from recent iron oolites from Indonesia (Heikoop et al., 1996) and the above findings are in general agreement with our suggestion of a positively fractionated shallow modern seawater composition. The following facts are in support of this assumption: 1) the most abundant form of Cr in oxygenated water is Cr(VI) species with smaller amounts but still analytically significant levels of Cr(III) species. Trivalent chromium is oxidized slowly by dissolved oxygen while manganese oxide is a strong catalyst for such oxidation (Van der Weijden and Reith, 1982). However, the low oceanic concentration of suspended MnO_2 makes this process rather unimportant and the distribution of dissolved Cr(III) and Cr(VI) species is probably kinetically controlled. 2) No detectable isotope exchange between soluble Cr(VI) and Cr(III) species at pH values of 5.5 and 7 is observed (Zink et al., 2010) over a timescale of days to weeks. This means that within such a time frame, the isotope composition of Cr(VI) in a natural system will not be influenced by equilibration with any Cr(III) and thus likely reveals the true extent of reduction. 3) The consistency between positively fractionated δ^{53}Cr values of modern seawater measured so far and shallow water concretions suggests that dissolved heavy Cr (inferably Cr(VI)) in shallow seawater is effectively conveyed into different chemical precipitates without a major change of its isotopic signature.

While the stripping mechanism for iron-rich chemical sediments is likely controlled by co-precipitation and adsorption of Cr(III) species which result from the effective oxidation of Fe^{2+} to Fe^{3+} and concomitant reduction of Cr^{6+} to Cr^{3+} during upwelling of Fe^{2+}-rich, hydrothermally-fed bottom waters into shallow water environments (Døssing et al., 2011; Frei et al., 2009; Pettine et al., 1998), the incorporation of Cr into carbonates remains to be investigated in detail, but Tang et al. (2007) revealed that Cr(VI) is readily co-precipitated with calcite as chromate (CrO_4^{2-}) species and that the concentration of Cr incorporated in calcite increases with increasing Cr concentration in solution. On the basis of these experimental studies, our data set (Table 1 and Fig. 5) implies that Cr(VI) concentrations in shallow seawater were elevated before and after the N1 δ^{13}C excursion (i.e. during warmer periods), and lowered during the cold period in which glaciers probably existed at higher latitudes.

Supported by the relationship between δ^{53}Cr values and Sr and Nd isotopes, respectively (Fig. 4 a–b; discussed below), the δ^{53}Cr values recorded in the carbonates across the N1 negative δ^{13}C excursion (Fig. 3) can be explained by a variable mixture of continentally derived, positively fractionated components with subaqueos-hydrothermally derived chromium inputs to the basin at the time of carbonate deposition. The positively fractioned values in carbonates deposited before and after the N1 negative δ^{13}C excursion show δ^{53}Cr values slightly lighter than modern seawater (δ^{53}Cr ~+0.5‰). A decrease to δ^{53}Cr values characterizing high-T magmatic rocks (δ^{53}Cr ~−0.12‰; Schoenberg et al. (2008)) is recorded in the lower part of unit B (the N1 negative δ^{13}C excursion) which implies that either the hydrothermal chromium input became dominant and/or that the input of positively fractionated chromium from the land was diminished. The correlated decrease of the δ^{53}Cr values during the N1 event with Cr concentrations (Fig. 5) however favors the interpretation that it is the diminishing riverine input with heavy δ^{53}Cr values causing this excursion rather than a higher hydrothermal input with light δ^{53}Cr values. In other words, the continental input of positively fractionated Cr contributed substantially to the overall Cr budget in shallow seawater at times when this input was effective, and that relatively lower Cr concentrations with a high-T isotopic signature prevailed during times when continental input was essentially prevented.

5.2. Chromium isotope fluctuations compared to those of other tracers

Carbonates from the Calera de Recalde deposited during the most pronounced negative (N1) δ^{13}C excursion show correlations with other isotope tracers commonly used to quantify hydrothermal vs. continental input into seawater. In Fig. 4a, the positive correlation between $^{87}Sr/^{86}Sr$ and δ^{53}Cr is pronounced and underlines that the chemical signals in these carbonates can be interpreted as mixing between two major sources with respect to Sr and Cr: The first, characterized by elevated $^{87}Sr/^{86}Sr$ ratios and positive δ^{53}Cr values, is consistent with a continentally-derived source. The second, characterized by lower $^{87}Sr/^{86}Sr$ ratios and low (negative) δ^{53}Cr values can be equated with a hydrothermal source, with Sr isotope signatures dominated by inputs of deep circulation of hydrothermal fluids from mid-ocean ridge hydrothermal systems, and with Cr that is compatible with high-temperature magmatic compositions (Schoenberg et al., 2008).

This continental–hydrothermal fluid mixing is also depicted by the inverse correlation ($R^2 = 0.9$) between εNd (570 Ma) and the δ^{53}Cr values (Fig. 4b). Whereas the continentally influenced seawater composition is characterized by more negative εNd and by positive δ^{53}Cr values, the hydrothermal influence is defined by less negative εNd and negative δ^{53}Cr values which closely match the δ^{53}Cr values of ~−0.12‰ for high-temperature magmatic systems (Schoenberg et al., 2008).

Data (Table 1) presented herein for the late Neoproterozoic carbonates of the ASG also reveal a correlation between Sm/Nd ratios (here expressed by the $^{147}Sm/^{144}Nd$ ratio) and εNd(570 Ma) values (diagram not shown here) The sensitivity of the Sm–Nd isotopic tracer system in chemical sediments to delineate and distinguish between different source inputs of REEs into ancient seawater has been demonstrated previously. Thus, for example, Sm–Nd isotopic relationships in BIFs from the ~3.7 Ga Isua Greenstone Belt (Western

Greenland) have been used by Frei and Polat (2007) to trace the compositional variations of seawater from which these BIFs were deposited. In their study, Sm–Nd isotopic relations on a layer-by-layer basis pointed to two REE sources controlling the back-arc basin depositional environment of the BIF, one being seafloor-vented hydrothermal fluids, the other being ambient surface seawater which reached its composition by erosion of parts of the protocrustal landmass. Similar relationships in younger, ~2.7 Gyr BIFs in Botswana were reported by Døssing et al. (2009).

Due to the relatively short residence times of Nd (200–10,000 years; Bertram and Elderfield (1993); Tachikawa et al. (1999)) and Cr (poorly constrained, estimated between 7000 and 40,000 years; (Campbell and Yeats, 1984; Van der Weijden and Reith, 1982)) one would expect to observe a well defined correlation between these two elements. The signatures most probably reflect rather local surface seawater conditions. In contrast, Sr is well-mixed (residence time of 2.4 Myr; Veizer, 1989) and fluctuations in Sr isotopic signatures in carbonates likely mirror a true global seawater signal. This discrepancy in residence times might explain the poorer correlations between δ^{53}Cr and εNd (570 Ma) with $^{87}Sr/^{86}Sr$ values of the carbonates studied (Fig. 4a,c). It might also explain that Sr isotope signatures remain low throughout P2 and even in following negative δ^{13}C excursion between P2 and P3 (Fig. 3).

Our study illustrates that the combination of redox sensitive tracers, such as exemplified by Cr isotopes, with more commonly used isotope tracers of lithophile elements (Sr and Sm–Nd) in carbonates may contribute to unravel the compositional fluctuations of ancient seawater and their relationships with climate change and evolving geodynamic processes which will directly influence the seawater archives. The fluctuations of Nd, Sr and Cr isotope data in the Calera de Recalde profile are compatible with a straightforward explanation of a decreased riverine input of these elements resulting from decreased continental erosion and/or decreased atmospheric oxygenation during a cold period with partial ice cover at higher latitudes.

5.3. Significance of Cr isotope fluctuations

The cause of the fluctuations in the input of positively fractionated Cr from the continent is a crucial question which needs to be addressed. A non-global glacial event was proposed (Gaucher and Poiré, 2009a; Gaucher et al., 2004b) to explain the δ^{13}C negative excursion N1 at the Calera de Recalde section, concomitant to significant sea-level drop as shown by sedimentary structures (Fig. 3). In such a scenario, chemical weathering on the continents would be impaired by low temperatures and ice cover, eventually leading to lower inputs of positively fractionated Cr to the oceans and thus diminished δ^{53}Cr values. This process could theoretically occur without significant changes in atmospheric oxygenation, analogous to Quaternary high-latitude glaciations. However, the following facts militate against glaciation-related processes being the sole cause of the negative δ^{53}Cr excursion:

(1) $^{87}Sr/^{86}Sr$ values begin to decrease well *before* (*ca.* 50 m stratigraphically, Fig. 3) the δ^{53}Cr negative excursion, and keep at their lowest values (0.7070, Fig. 3; Table 1) during the overlying positive δ^{53}Cr excursion. According to the model presented by Jacobsen and Kaufman (1999) the decrease of $^{87}Sr/^{86}Sr$ ratios caused by global ice cover should start with the beginning of the glacial event and not before.

(2) εNd shows a similar behavior, decreasing from −16.5 to −13.5 at least 70 m below the crossover from positive to negative δ^{13}C and 30 m below the first sedimentological evidence of sea-level fall (Fig. 3). It is worth noting that negative δ^{13}C values usually precede the first glacial deposits in Neoproterozoic glaciations by as much as 0.6 Myr (Halverson et al., 2002).

(3) Since the Arroyo del Soldado basin was ice-free during deposition of the Polanco Formation, there is no straightforward explanation of why the water column should become anoxic at the transition from the P1 to the N1 excursion, as demonstrated by V/Th ratios (Velasquez, 2010).

Taken together, the data show that glaciation alone cannot account for the observed negative δ^{53}Cr excursion. A second mechanism capable of altering the input of positively fractionated Cr to the oceans is oxygen concentration in the atmosphere. Indeed, it is noteworthy that δ^{53}Cr mirrors δ^{13}C (Fig. 3), which can be taken as a measure of photosynthetic O_2 production. This mechanism implies that δ^{13}C was largely controlled by bioproductivity changes (Gaucher, 2000; Gaucher et al., 2004b; Velasquez, 2010) and not by other factors such as organic matter preservation. Furthermore, redox changes in the water column can be easily explained: during high-bioproductivity phases (e.g. P1, P2 excursions) high amounts of oxygen would be released by phytoplankton to the water column and atmosphere, leading to oxygenated conditions. At the end of high-bioproductivity stages, the large amount of organic matter accumulated in the ocean would exhaust dissolved oxygen, causing widespread anoxia. Anoxic conditions would persist throughout the negative δ^{13}C excursions due to diminished photosynthetic activity and oxygen production as indicated by the near canonic mantle δ^{13}C values.

As pointed out by various authors (Gaucher, 2000; Gaucher et al., 2004b; Kaufman et al., 1997), the above scenario would only be feasible if enhanced hydrothermal activity provided (1) enough reductants to keep the deep ocean anoxic, and (2) large amounts of nutrients, such as Fe, to fuel the high-productivity intervals. Ferruginous conditions indeed dominated the Ediacaran ocean, as shown by iron speciation studies (Canfield et al., 2008). In the Polanco Formation, $^{87}Sr/^{86}Sr$ and εNd values show that hydrothermal inputs increased remarkably during deposition of the upper unit A and units B–C. If so, why does δ^{13}C fluctuate between positive and negative values (upper P1, N1 and P2 excursions) despite continuously low $^{87}Sr/^{86}Sr$ values? We envisage CO_2 limitation (Riebesell et al., 1993) as a mechanism capable of triggering a negative δ^{13}C excursion in an otherwise nutrient-rich ocean. If indeed the biota became CO_2-limited at the P1–N1 transition it means that atmospheric CO_2 levels sank dramatically, which is consistent with global cooling and glaciation. Modern eukaryotic phytoplankton is severely limited below 10 μM CO_2 (*ca.* 230 ppm atmospheric CO_2; Riebesell et al. (1993)). Hein and Sand-Jensen (1997) reported a 25% decrease in primary productivity at reduced CO_2 concentrations of 3 μM in the Atlantic Ocean. CO_2 atmospheric concentrations between 80 and 250 ppm may have been required for Neoproterozoic low-latitude glaciation (Godderis et al., 2007). Thus, CO_2 limitation is consistent with the occurrence during the N1 negative excursion of a glacial event affecting higher latitudes (Gaucher and Poire, 2009; Gaucher et al., 2004b). Therefore, in our preferred scenario, glaciation is not the cause of negative δ^{13}C and δ^{53}Cr excursions, but only one more consequence of a tectonically-driven, biologically mediated system. In fact, glaciation acts as an amplifier of δ^{53}Cr signals, lowering chemical weathering rates of continental crust during times of low atmospheric oxygen concentrations.

Summing up, we envisage that final rifting of Rodinia and/or a mantle plume events led to higher hydrothermal inputs to the ocean, initially fertilizing the ocean and causing enhanced bioproductivity and oxygenation of the surface environments (P1 excursion). Drawdown of atmospheric CO_2 led to a collapse of bioproductivity and photosynthetic oxygen production, anoxia and ultimately glaciation (N1 excursion). Diminished bioproductivity during the glacial event would allow for CO_2 build up from volcanic outgassing, enabling once again a bioproductivity burst, renewed oxygenation and ice retreat (P2 excursion).

5.4. Correlation of the Arroyo del Soldado Group with other carbonate successions

The positive and negative $\delta^{13}C$ fluctuations recorded in the ASG have been correlated with fluctuations in the Corumbá Group (Mato Grosse do Sul, Brazil; (Boggiani et al., 2010; Gaucher et al., 2003)), in the Nama and Witvlei Groups (Namibia; (Fölling and Frimmel, 2002; Grotzinger et al., 1995; Kaufman et al., 1991)) and in the Windermere Group (Canada; (Narbonne et al., 1994)), and tentatively also with profiles in the Nafun and Ara Groups (Oman;(Amthor et al., 2003; Brasier et al., 2000)). Following the Gaskiers glaciation at 583 Ma, three negative $\delta^{13}C$ excursions have been identified, one ending at *ca.* 551 Ma (Shuram–Wonoka anomaly), a second at *ca.* 547 Ma separating the Kuibis and Schwarzrand Subgroups in the Nama Group and the third at the Ediacaran–Cambrian boundary. The two older negative $\delta^{13}C$ excursions have been correlated with the N1 and N2 excursion in the ASG (Gaucher et al., 2004b) and are well correlated with respective fluctuations in the Tamengo Formation (Corumbá Group, Brazil; (Boggiani et al., 2010)). They have been interpreted to be related to glacial events of high-latitude and not global nature. Boggiani et al. (2010) correlated the oldest (N1) negative $\delta^{13}C$ excursions in the ASG and Tamengo Formation with the Shuram excursion in Oman and the excursion recorded in the transition between the Port Noloth and Nama Groups in Namibia. Future studies will have to include Cr isotope data on carbonates from these successions to build a record of $\delta^{53}Cr$ variations of the Ediacaran glacial period.

5.5. Cr isotopes in carbonates and the "link" to seawater

Collectively, the fluctuations of Cr isotope values in the Polanco Formation support a glacio-marine scenario as proposed by Gaucher et al. (2004b) to explain the $\delta^{13}C$ N1 negative excursion and its chemostratigrahical correlates in Namibia and Brazil (Boggiani et al., 2010; Gaucher et al., 2003). In such a scenario, sea-level fall and concomitant reduction of the size of sedimentary basins as indicated by sedimentological observations (Gaucher et al., 2004b), potentially caused by glaciation of high latitude regions of the Earth at ~560 Ma, would have occurred during negative $\delta^{13}C$ excursions. During such cold periods, low CO_2 concentrations greatly diminished photosynthetic primary productivity. Ice cover, diminished chemical weathering and lower photosynthetic oxygen production contributed to the return of Cr isotope signals to high-T magmatic signatures during these periods. To what degree the $\delta^{53}Cr$ values in carbonates can be linked to atmospheric conditions (most importantly to oxygen pressures prevailing during weathering periods) depends on a number of parameters, such as 1) the contribution of released Cr from the continents relative to the total Cr budgets on land which controls the fractionation of released Cr(VI), 2) effects of Cr isotope fractionation in reductive processes during transport which could transform mobile Cr(VI) back to immobile Cr(III), thereby potentially affecting the isotopic composition of the remaining Cr(VI) in solution (essentially rendering the isotopic composition of remaining mobile Cr(VI) even heavier), 3) biological processes and photochemical reactions in the water column (Connelly et al., 2006) and, 4) potential fractionation effects during solid solution and/or adsorptive sequestration of Cr into/onto precipitating carbonates. In spite of the incomplete understanding of mechanisms controlling Cr fractionation in the natural Cr cycle, the outcome of our study, namely the systematic correlation of the *relative* fluctuations of $\delta^{53}Cr$ values with other parameters used as monitors for source-dependent compositional changes of ancient seawater, may inspire future research aiming at developing the Cr isotope system as an additional chemostratigraphic tool for investigating redox processes in ancient marine successions throughout Earth's history.

6. Conclusions

Carbon, Cr, Sr and Sm–Nd isotope chemostratigraphy revealed a remarkable pattern of covariation in the Polanco Formation (Calera de Recalde Syncline, Uruguay), which was deposited during the late Ediacaran as shown by biostratigraphy and $\delta^{13}C$ chemostratigraphy. The studied sequence comprises a pronounced negative $\delta^{13}C$ excursion (with values as low as −4.5‰) in the carbonatic Polanco Formation which overlies the siliciclastic Yerbal Formation of the ASG in Uruguay. The latter contains iron-rich cherts and thin BIF horizons from which strongly fractionated, positive $\delta^{53}Cr$ signatures of up to +4.9‰ have been reported (Frei et al., 2009). The negative $\delta^{13}C$ excursion has been correlated in previous studies with the Shuram–Winoka anomaly, reported from several Neoproterozoic successions worldwide.

$\delta^{53}Cr$ varies between positive values up to +0.29‰ (before and after the negative $\delta^{13}C$ excursion) and −0.17‰ (within the negative $\delta^{13}C$ excursion) indicating a positively fractionated seawater pool and one characterized by values typical of high-temperature magmatic derivatives.

$\delta^{53}Cr$ values correlate with $^{87}Sr/^{86}Sr$ and εNd(570 Ma) values and with Cr concentrations of the carbonates such that the variations can be explained by mixing of deep-water, hydrothermal fluids characterized by lower $^{87}Sr/^{86}Sr$ ratios, less negative εNd(570 Ma) values, and smaller Cr concentrations with shallow seawater characterized by elevated $^{87}Sr/^{86}Sr$ ratios, more negative εNd(570 Ma) values, and by elevated Cr concentrations typically characterizing a continental crust origin.

Mirroring of the $\delta^{13}C$ negative excursion by $\delta^{53}Cr$ values is seen as a consequence of changes in bioproductivity. We envisage a photosynthetic oxygenation of shallow marine environments during high bioproductivity stages (positive $\delta^{13}C$ excursions) fueled by high availability of nutrients. The transition from the underlying positive $\delta^{13}C$ carbonates into the negatively fractionated $\delta^{13}C$ carbonates defining the pronounced negative excursion thereby indicates a change from oxic to anoxic surface waters. The concomitant change from positive to negative $\delta^{53}Cr$ values is interpreted as being produced by the same process. A massive CO_2 drawdown during high-bioproductivity periods and eventual CO_2 limitation of the biota was a key factor eventually leading to a collapse of bioproductivity, exhaustion of dissolved oxygen in surface waters and widespread anoxia. CO_2 drawdown ultimately led to a glacial event as indicated by sea-level fall and associated negative $\delta^{13}C$ values, possibly in a similar manner to older Neoproterozoic, low-latitude glaciations. The fact that $^{87}Sr/^{86}Sr$ values, despite $\delta^{13}C$ fluctuations, remain low (indicative of a strong hydrothermal input) implies that CO_2 limitation may be the cause of negative $\delta^{13}C$ and $\delta^{53}Cr$ excursions in otherwise nutrient rich late Ediacaran oceans, and that glaciation is only one more consequence of a tectonically-driven, biologically mediated system. Glaciation alone cannot account for the changes observed in $\delta^{53}Cr$, which is tightly linked to $\delta^{13}C$ secular variations and thus photosynthetic oxygen production. In such a scenario, glaciation acts as an amplifier of $\delta^{53}Cr$ signals by preventing Cr inputs from the continents through diminished chemical weathering due to the partial ice cover on land.

We therefore propose that chromium isotopes in marine carbonates are a sensitive tracer of weathering of the continental crust as well as of hydrothermal input into the basin. Chemical weathering is more effective during warm periods typically following deglaciation because of a likely increase of atmospheric oxidation. This enables mobilization of lithogenically bound Cr(III) by its oxidation to heavy Cr(VI) and its transport into the shallow seawater where the signal is conveyed into the chemical precipitates. Chromium isotopes in marine carbonates, similar to BIFs, have the potential to monitor atmospheric fluctuations through time, particularly those that occurred during periods dominated by ice age/greenhouse-type climatic changes.

Acknowledgments

We thank Toni Larsen for the help in ion chromatographic separation of chromium, and Toby Leeper for keeping the mass spectrometer in perfect state. We are grateful for partial funding of the project by FNU grant 272-07-0244 to RF, and for stimulating discussions with members of the Nordic Center for Earth Evolution (NordCEE). Jeff Heikoop has kindly provided the recent iron oolite sample from Indonesia. We thank three anonymous reviewers for their constructive comments which significantly improved our initial manuscript.

Appendix A. Supplementary data

Supplementary data to this article can be found online at doi:10.1016/j.epsl.2011.10.009.

References

Amthor, J.E., Grotzinger, J.P., Schröder, S., Bowring, S.A., Ramezani, J., Martin, M.W., Matter, A., 2003. Extinction of Cloudina and Namacalthus at the Precambrian–Cambrian boundary in Oman. Geology 31, 431–434.

Bain, D.J., Bullen, T.D., 2005. Chromium isotope fractionation during oxidation of Cr(III) by manganese oxides. Geochim. Cosmochim. Acta 69, A212.

Berna, E.C., Johnson, T.M., Makdisi, R.S., Basui, A., 2010. Cr stable isotopes as indicators of Cr(VI) reduction in groundwater: a detailed time-series study of a point-source plume. Environ. Sci. Technol. 44, 1043–1048.

Bertram, C.J., Elderfield, H., 1993. The geochemical balance of the rare-earth elements and neodymium isotopes in the oceans. Geochim. Cosmochim. Acta 57, 1957–1986.

Boggiani, P.C., Gaucher, C., Sial, A.N., Babinski, M., Simon, C.M., Riccomini, C., Ferreira, V.P., Fairchild, T.R., 2010. Chemostratigraphy of the Tamengo Formation (Corumbá Group, Brazil): a contribution of the calibration of the Ediacaran carbon-isotope curve. Precambrian Res. 182, 382–401.

Bonnand, P., Parkinson, I.J., James, R.H., Fehr, M., Connelly, D.P., 2010. Cr isotopic compostion of modern carbonates and seawater. American Geophysical Union, Fall Meeting, San Francisco.

Bonnand, P., Parkinson, I.J., James, R.H., Karjalainen, A.-M., Fehr, M.A., 2011. Accurate and precise determination of stable Cr isotope compositions in carbonates by double spike MC-ICP-MS. J. Anal. At. Spectrom.. doi:10.1039/c0ja00167h

Bossi, J., Cingolani, C., 2009. Extension and general evolution of the Rio de la Plata Craton. In: Gaucher, C., Halverson, A.N., Frimmel, H.E. (Eds.), Neoproterozoic–Cambrian Tectonics, Global Change and Evolution: a Focus on Southwestern Gondwana. Elsevier, Amsterdam, pp. 73–85.

Bossi, J., Gaucher, C., 2004. The Cuchilla Dionisio Terrane, Uruguay: an allochthonous block accreted in the Cambrian to SW-Gondwana. Gondwana Res. 7, 661–674.

Brasier, M., McCarron, G., Tucker, R., Leather, J., Allen, P., Shields, G., 2000. New U–Pb zircon dates for the Neoproterozoic Ghubrah glaciation and for the top of the Huqf Supergroup, Oman. Geology 28, 175–178.

Campbell, J.A., Yeats, P.A., 1984. Dissolved chromium in the northwest Atlantic Ocean. Earth Planet. Sci. Lett. 53, 427–433.

Canfield, D.E., Poulton, S.W., Knoll, A.H., Narbonne, G.M., Ross, G., Goldberg, T., Strauss, H., 2008. Ferruginous conditions dominated later Neoproterozoic deep-water chemistry. Science 321, 949–952.

Connelly, D.P., Statham, P.J., Knap, A.H., 2006. Seasonal changes in speciation of dissolved chromium in the surface Sargasso Sea. Deep-Sea Res. I 53, 1975–1988.

Døssing, L.N., Frei, R., Stendal, H., Mapeo, R.B.M., 2009. Characterization of enriched lithospheric mantle components in 2.7 Ga banded iron formations: an example from the Tati Greenstone Belt, Northeastern Botswana. Precambrian Res. 172, 334–356.

Døssing, L.N., Dideriksen, K., Stipp, S.L.S., Frei, R., 2011. Reduction of hexavalent chromium by ferrous iron: a process of chromium isotope fractionation and its relevance to natural environments. Chem. Geol. 285, 157–166.

Ellis, A.S., Johnson, T.M., Bullen, T.D., 2002. Chromium isotopes and the fate of hexavalent chromium in the environment. Science 295, 2060–2062.

Fölling, P.G., Frimmel, H.E., 2002. chemostratigraphic correlation of carbonate successions in the Gariep and Saldania Belts, Namibia and South Africa. Basin Res. 14, 69–88.

Frei, R., Polat, A., 2007. Source heterogeneity for the major components of similar to 3.7 Ga banded iron formations (Isua Greenstone Belt, Western Greenland): tracing the nature of interacting water masses in BIF formation. Earth Planet. Sci. Lett. 253, 266–281.

Frei, R., Gaucher, C., Poulton, S.W., Canfield, D.E., 2009. Fluctuations in Precambrian atmospheric oxygenation recorded by chromium isotopes. Nature 461, 250–253.

Gaucher, C., 2000. Sedimentology, paleontology and stratigraphy of the Arroyo del Soldado Group (Vendian to Cambrian; Uruguay). Beringeria 26, 1–120.

Gaucher, C., Poire, D.G., 2009. Paleoclimatic events. Neoproterozoic–Cambrian evolution of the Rio de la Plata Palaeocontinent. In: Gaucher, C., Sial, A.N., Halverson, G.P., Frimmel, H.E. (Eds.), Neoproterozoic–Cambrian Tectonics, Global Change and Evolution: A Focus on Southwestern Gondwana. Development in Precambrian Geology. Elsevier, pp. 123–130.

Gaucher, C., Poiré, D.G., 2009a. Biostratigraphy. Neoproterozoic–Cambrian Evolution of the Rio de la Plata Palaeocontinent. In: Gaucher, C., Sial, A.N., Halverson, G.P., Frimmel, H.E. (Eds.), Neoproterozoic–Cambrian Tectonics, Global Change and Evolution: A focus on Southwestern Gondwana. Elsevier, pp. 103–114.

Gaucher, C., Poiré, D.G., 2009b. Paleoclimatic events. Neoproterozoic–Cambrian evolution of the Rio de la Plata Palaeocontinent. In: Gaucher, C., Sial, A.N., Halverson, G.P., Frimmel, H.E. (Eds.), Neoproterozoic–Cambrian Tectonics, Global Change and Evolution: A Focus on Southwestern Gondwana. Development in Precambrian Geology. Elsevier, pp. 123–130.

Gaucher, C., Boggiani, P.C., Sprechmann, P., Sial, A.N., Fairchild, T., 2003. Integrated correlation of the Vendian to Cambrian Arroyo del Soldado and Corumba Groups (Uruguay and Brazil): Palaeogeographic, palaeoclimatic and palaeobiologic implications. Precambrian Res. 120, 241–278.

Gaucher, C., Chiglino, L., Pecoits, E., 2004a. Southernmost exposures of the Arroyo del Soldado Group (Vendian to Cambrian, Uruguay): Palaeogeographic implications for the amalgamation of W-Gondwana. Gondwana Res. 7, 701–714.

Gaucher, C., Sial, A.N., Blanco, G., Sprechmann, P., 2004b. Chemostratigraphy of the lower Arroyo del Soldado Group (Vendian, Uruguay) and palaeoclimatic implications. Gondwana Res. 7, 715–730.

Gaucher, C., Poire, D.G., Gomez Peral, L., Chiglino, L., 2005. Litoestratigrafia, bioestratigrafia y correlaciones de las sucesiones sedimentarias Neoproterozoico–Cambrico del Craton del Rio de la Plata (Uruguay y Argentina). Lat. Am. J. Sediment. Basin Anal. 12, 145–160.

Gaucher, C., Sial, A.N., Ferreira, V.P., Pimentel, T.M., Chiglino, M., Sprechmann, P., 2007. Chemostratigraphy of the Cerro Victoria Formation (Lower Cambrian, Uruguay): evidence for progressive climate stabilization across the Precambrian–Cambrian boundary. Chem. Geol. 237, 28–46.

Gaucher, C., Blanco, G., Chiglino, L., Poire, D.G., Germs, D.J.G., 2008a. Acritarchs of Las Ventanas Formation (Ediacaran, Uruguay): implications for the timing of coeval rifting and glacial events in western Gondwana. Gondwana Res. 13, 488–501.

Gaucher, C., Finney, S.C., Poire, D.G., Valencia, V.A., Grove, M., Blanco, G., Pamoukaghlian, L.G., Peral, L.G., 2008b. Detrital zircon ages of Neoproterozoic sedimentary successions in Uruguay and Argentina: insights into the geological evolution of the Rio de la Plata Craton. Precambrian Res. 167, 150–170.

Gaucher, C., Sial, A.N., Poire, D.G., Gomez Peral, L., Ferreira, V.P., Pimentel, M.M., 2009. Chemostratigraphy, Neoproterozoic–Cambrian evolution of the Rio de la Plata Palaeocontinent. In: Gaucher, C., Sial, A.N., Halverson, G.P., Frimmel, H.E. (Eds.), Neoproterozoic–Cambrian tectonics, Global Change and Evolution: A Focus on Southwestern Gondwana. Developments in Precambrian Geology. Elsevier, Amsterdam, pp. 115–122.

Godderis, Y., Donnadieu, Y., Dessert, C., Dupre, B., Fluteau, F., Francois, L.M., Meert, J., Nedelec, A., Ramstein, G., 2007. Coupled modeling of global carbon cycle and climate in the Neoproterozoic: links between Rodinia breakup and major glaciations. C. R. Geosci. 339, 212–222.

Grotzinger, J.P., Bowring, S.A., Saylor, B.Z., Kaufman, A.J., 1995. Biostratigraphic and geochronologic constraints on early animal evolution. Science 270, 598–604.

Halverson, G.P., Hoffman, P.F., Schrag, D.P., Kaufman, A.J., 2002. A major perturbation of the carbon cycle before the Ghaub glaciation (Neoporoterozoic) in Namibia: prelude to snowball Earth. Geochem. Geophys. Geosyst. 3, 1–24.

Heikoop, J.M., Tsujita, C.J., Risk, M.J., Tomascik, T., Mah, A.J., 1996. Modern iron ooids from a shallow-marine volcanic setting: Mahengetang, Indonesia. Geology 24, 759–762.

Hein, M., Sand-Jensen, K., 1997. CO_2 increases oceanic primary production. Nature 388, 526–527.

Horowitz, E.P., Chiarizia, R., Dietz, M.L., 1992. A novel strontium-selective extraction chromatographic resin. Solvent Extr. Ion Exch. 10, 313–336.

Izbicki, J.A., Ball, J.W., Bullen, T.D., Sutley, S.J., 2008. Chromium, chromium isotopes and selected elements, western Mojave Desert, USA. Appl. Geochem. 23, 1325–1352.

Jacobsen, S.B., Kaufman, A.J., 1999. the Sr, C and O isotopic evolution of Neoproterozoic seawater. Chem. Geol. 161, 37–57.

Johnston, D.T., Poulton, S.W., Dehler, C., Porter, S., Husson, J., Canfield, D.E., Knoll, A.H., 2010. An emerging picture of Neoproterozoic ocean chemistry: insights from the Chuar Group, Grand Canyon, USA. Earth Planet. Sci. Lett. 290, 64–73.

Kalsbeek, F., Frei, R., 2010. Geochemistry of Precambrian sedimentary rocks used to solve stratigraphical problems: an example from the Neoproterozoic Volta basin, Ghana. Precambrian Res. 176, 65–76.

Kaufman, A., Hayes, J.M., Knoll, A.H., Germs, G.J.B., 1991. Isotopic compositions of carbonates and organic carbon from upper Proterozoic successions in Namibia: stratigraphic variation and the effects of diagenesis and metamorphism. Precambrian Res. 49, 301–327.

Kaufman, A.J., Knoll, A.H., Narbonne, G.M., 1997. Isotopes, ice ages, and terminal Proterozoic earth history. Proc. Natl. Acad. Sci. U. S. A. 94, 6600–6605.

Kim, J.G., Dixon, J.B., Chusuei, C.C., Deng, Y.J., 2002. Oxidation of crhomium(III) to (VI) by manganese oxides. Soil Sci. Soc. Am. J. 66, 306–315.

Mallmann, G., Chemale, F., Avila, J.N., Kawashita, K., Armstrong, R.A., 2007. Isotope geochemistry and geochronology of the Nico Perez terrane, Rio de la Plata craton, Uruguay. Gondwana Res. 12, 489–508.

Narbonne, G.M., Kaufmann, A.J., Knoll, A.H., 1994. Integrated chemostratigraphy of the Windermere supergroup, northwestern Canada: implications for Neoproterozoic correlations and the early evolution of animals. Geol. Soc. Am. Bull. 106, 1281–1292.

Oyantcabal, P., Siegesmund, S., Wemmer, K., Presnyakov, S., Layer, P., 2009. Geochronological constraints on the evolution of the southern Dom Feliciano Belt (Uruguay). J. Geol. Soc. 166, 1075–1084.

Oze, C., Bird, D.K., Fendorf, S., 2007. Genesis of hexavalent chromium from natural sources in soil and groundwater. Proc. Natl. Acad. Sci. 104, 6544–6549.

Pettine, M., D'Ottone, L., Campanella, L., Millero, F.J., Passino, R., 1998. The reduction of chromium (VI) by iron (II) in aqueous solutions. Geochim. Cosmochim. Acta 62, 1509–1519.
Riebesell, U., Wolf-Gladrow, D.A., Smetacek, V., 1993. Carbon dioxide limitation of marine phytoplankton growth rates. Nature 361, 249–251.
Schoenberg, R., Zink, S., Staubwasser, M., von Blanckenburg, F., 2008. The stable Cr isotope inventory of solid Earth reservoirs determined by double spike MC-ICP-MS. Chem. Geol. 249, 294–306.
Tachikawa, K., Jeandel, C., Roy-Barman, M., 1999. A new approach to the Nd residence time in the ocean: the role of atmospheric inputs. Earth Planet. Sci. Lett. 170, 433–446.
Tanaka, T., Togashi, S., Kamioka, H., Amakawa, H., Kagami, H., Hamamoto, T., Yuhara, M., Orihashi, Y., Yoneda, S., Shimizu, H., Kunimaru, T., Takahashi, K., Yanagi, T., Nakano, T., Fujimaki, H., Shinjo, R., Asahara, Y., Tanimizu, M., Dragusanu, G., 2000. JNdi1: a neodymium isotope reference in consistency with LaJolla neodymium. Chem. Geol. 168, 279–281.
Tang, Y., Elzinga, E.J., Lee, Y.J., Reeder, R.J., 2007. Coprecipitation of chromate with calcite: batch experiments and X-ray absorption spectroscopy. Geochim. Cosmochim. Acta 71, 1480–1493.
Van der Weijden, C.H., Reith, M., 1982. Chromium(III) Chromium(VI) interconversions in seawater. Mar. Chem. 11, 565–572.
Veizer, J., 1989. Strontium isotopes in the seawater through time. Annu. Rev. Earth Planet. Sci. 17, 141–167.
Velasquez, M., 2010. Environmental Changes in the Aftermath of Neoproterozoic Glaciations: A Biochemical Study of Sediments from SW-Gondwana. Université de Lausanne, Lausanne. 200 pp.
Zink, S., Schoenberg, R., Staubwasser, M., 2010. Isotopic fractionation and reaction kinetics between Cr(III) and Cr(VI) in aqueous media. Geochim. Cosmochim. Acta 74, 5729–5745.